On the Use of Directional Importance Sampling for Reliability-Based Design and Optimum Design Sensitivity of Linear Stochastic Structures

Danko J. Jerez[a,*], Héctor A. Jensen[b], Marcos A. Valdebenito[c], Mauricio A. Misraji[d], Franco Mayorga[e], Michael Beer[a,f,g]

[a] *Institute for Risk and Reliability, Leibniz Universität Hannover, Callinstr. 34, 30167 Hannover, Germany*
[b] *Departamento de Obras Civiles, Universidad Técnica Federico Santa María, Avda. España 1680, Valparaíso 2390123, Chile*
[c] *Faculty of Engineering and Sciences, Universidad Adolfo Ibáñez, Av. Padre Hurtado 750, Viña del Mar 2562340, Chile*
[d] *Consulting Engineer, Valparaíso, Chile*
[e] *Department of Structural Engineering, University of California San Diego, Gilman Drive 9500, La Jolla 92093, California, United States*
[f] *International Joint Research Center for Engineering Reliability and Stochastic Mechanics, Tongji University, 1239 Siping Road, Shanghai 200092, P.R. China*
[g] *Institute for Risk and Uncertainty and School of Engineering, University of Liverpool, Peach Street, Liverpool L69 7ZF, UK*

Abstract

This contribution focuses on reliability-based design and optimum design sensitivity of linear dynamical structural systems subject to Gaussian excitation. Directional Importance Sampling (DIS) is implemented for reliability assessment, which allows to obtain first-order derivatives of the failure probabilities as a byproduct of the sampling process. Thus, gradient-based solution schemes can be adopted by virtue of this feature. In particular, a class of feasible-direction interior point algorithms are implemented to obtain optimum designs, while a direction-finding approach is considered to obtain optimum design sensitivity measures as a post-processing step of the optimization results. To show the usefulness of the approach, an example involving a building structure is studied. Overall, the reliability sensitivity analysis framework enabled by DIS provides a potentially useful tool to address a practical class of design optimization problems.

Keywords: Structural design, First excursion probability, Directional Importance Sampling, Optimum design sensitivity, Linear structures, Gaussian loading, Interior point algorithm

1. Introduction

The design of safe and cost-effective structures to satisfy public and private needs is one of the most classical tasks in civil engineering. In this regard, structural systems are usually required to be optimum with respect to a given criterion while complying with a set of design conditions

[1]. Moreover, appropriate design procedures must take into account all relevant uncertainties about the system under consideration, as they can significantly affect the expected structural performance of final designs [2]. Especially relevant are uncertainties in environmental dynamical excitations, such as wind effects or earthquakes, which are commonly modeled by means of stochastic processes [3, 4, 5, 6, 7, 8, 9, 10, 11]. In this setting, reliability-based optimization (RBO) provides a realistic and rational framework for structural design which explicitly accounts for the uncertainties during the design process [12, 13].

RBO problems are usually formulated as the minimization of an objective function subject to both standard design requirements and reliability constraints. In structural dynamics applications, reliability is measured by means of first-passage probabilities. Some reliability analysis techniques that have been used in this context include, e.g., the Wiener path integral [14], statistical linearization [15], and advanced simulation techniques [16, 17, 18, 19, 20, 21]. In general, the choice of a solution method depends on the particular characteristics of the problem at hand. The reader is referred to [22] for a recent overview on RBO methods for structural dynamical systems under stochastic excitation.

Special attention is directed to the optimal design of linear structures subject to Gaussian excitation under constraints on first-passage probabilities. This type of problems arises, e.g., when requirements on serviceability conditions are considered [23, 24]. Several specialized approaches have been reported to address this particular class of problems. A stochastic search method is proposed in [18], which relies on the nested implementation of advanced simulation techniques to explore the design space and evaluate the reliability constraints. An adaptive scheme to allocate computational efforts is integrated for improved numerical efficiency. Alternatively, a sequential optimization approach is presented in [19], where failure probability functions are locally approximated using sensitivity information. It is noted that the previous methods use simulation techniques to evaluate the reliability constraints in a direct manner, without any approximation at the stochastic response level. On the other hand, the sequential optimization approaches presented in [25, 26, 27, 28] mainly rely on approximation schemes for (i) peak responses, (ii) failure probability functions, and (iii) the second-order statistics of the different responses of interest. These methods have proved effective in applications involving uncertain linear systems and high-dimensional design spaces. Approximations of the peak responses are formulated either using peak factors [25], the so-called auxiliary variable vector approach [26], or parametrized distributions [28]. In addition, for demand functions involving more than one response, reliability constraints are approximated with kriging metamodels for the so-called inverse reliability constraints [27], or by assuming the failure probability as proportional to the sum of its corresponding individual component-level failure probabilities [28]. Usually, the computation of the mean values and standard deviations of all responses of interest at any given design is required by these formulations. To this end, surrogates based on direct Monte Carlo simulation results from the previous candidate design are used. Even though all previous approaches have proved effective in a variety of applications, it is believed that there is still room for further developments in this area, particularly in the effective and efficient integration of specialized sampling methods in RBO procedures.

Several stochastic simulation techniques especially tailored to the reliability assessment of linear structures under Gaussian loading have been proposed. These include Efficient Importance Sampling [29], Domain Decomposition Method [30], Multidomain Line Sampling [31], and Directional Importance Sampling (DIS) [32]. These methods exploit the linear relationship between the structural responses and the set of basic random variables [33] to reduce the variability of failure probability estimates. In this work, DIS [32] is adopted to evaluate the reliability constraints. Further, this method also provides estimates of the first-order derivatives of the failure probability by reusing the sampling results [34]. As a result, sensitivities with respect to design variables and general model parameters can be obtained as a post-processing step of reliability assessment. This feature is particularly advantageous for the treatment of RBO problems, since suitable gradient-based solution schemes can be adopted.

It is the objective of this work to implement DIS as a general reliability and sensitivity assessment framework to treat RBO problems involving linear structural systems under Gaussian excitation. First-order solution schemes are adopted not only to identify optimal designs, but also to assess their sensitivity. On the one hand, a sequential optimization method based on a class of feasible-direction interior point algorithms [35, 36] is adopted to solve the RBO problem. This scheme provides a sequence of feasible designs with improving objective values, which is advantageous for practical purposes. Further, full reliability assessment at only few designs is usually required by this method. On the other hand, a direction-finding technique [37] is implemented to evaluate the sensitivity of optimum designs with respect to model parameter perturbations. This analysis is performed as a post-process of the optimization results, which allows to obtain a deeper understanding of final solutions with reduced computational efforts. Numerical results suggest that DIS represents a potentially useful tool for the treatment of a class of RBO problems.

The structure of this contribution is as follows. Section 2 formulates the problems of interest. The main ideas of Directional Importance Sampling are summarized in Section 3, whereas Section 4 discusses the enabled reliability sensitivity assessment framework. Section 5 describes the first-order solution schemes adopted for RBO and optimum design sensitivity assessment. A numerical example is presented in Section 6 to illustrate the applicability of the proposed framework. The paper closes with some conclusions and final remarks.

2. Formulation of the problem

The class of reliability-based design optimization problems of interest can be stated as

$$\begin{aligned} \min_{\mathbf{x}} \quad & f(\mathbf{x}) \\ \text{s.t.} \quad & r_j(\mathbf{x}) \leq 0, \quad j = 1, \ldots, n_r \\ & g_j(\mathbf{x}) \leq 0, \quad j = 1, \ldots, n_g \end{aligned} \tag{1}$$

where $\mathbf{x} \in \mathbb{R}^{n_x}$ denotes a vector of continuous design variables, $f(\mathbf{x})$ is the objective function, $r_j(\mathbf{x}) \leq 0, j = 1, \ldots, n_r$ characterize n_r constraints on structural reliability, and $g_j(\mathbf{x}) \leq 0, j = 1, \ldots, n_g$ represent n_g standard constraints. Typical objective functions include construction or maintenance costs, total weight, etc. Reliability constraints represent design conditions formulated in terms of reliability measures, such as the verification of serviceability limit states. On the other hand, standard constraints are requirements that do not involve structural reliability assessment, including geometric design needs, material availability, etc. Note that the side constraints on the design variables, i.e., $x_i^L \leq x_i \leq x_i^U, i = 1, \ldots, n_x$ with x_i^L and x_i^U the lower and upper bounds on x_i, respectively, are contained in the set of n_g standard constraints. Finally, in the context of this contribution, the objective function does not involve reliability assessment and, therefore, it is assumed that the objective and standard constraint functions are computationally inexpensive to evaluate.

2.1. Mechanical modeling

The structural dynamical systems of interest are characterized by means of linear, elastic and classically damped multi-degree-of-freedom models, which satisfy the equation of motion

$$\mathbf{M}(\mathbf{x})\ddot{\mathbf{y}}(t,\mathbf{x},\boldsymbol{\theta}) + \mathbf{C}(\mathbf{x})\dot{\mathbf{y}}(t,\mathbf{x},\boldsymbol{\theta}) + \mathbf{K}(\mathbf{x})\mathbf{y}(t,\mathbf{x},\boldsymbol{\theta}) = \mathbf{q}(\mathbf{x})p(t,\boldsymbol{\theta}) \tag{2}$$

where $\ddot{\mathbf{y}}$, $\dot{\mathbf{y}}$, and $\mathbf{y}$ are, respectively, the acceleration, velocity, and displacement vectors of dimension n_y; the matrices $\mathbf{M}$, $\mathbf{C}$, and $\mathbf{K}$ characterize the mass, damping and stiffness properties of the structure; $\mathbf{q}$ is a vector coupling the excitation p with the structural degrees of freedom; and $\boldsymbol{\theta}$ is the vector of basic random variables.

2.2. Stochastic Gaussian excitation

The dynamic load p of duration T is characterized as a discrete Gaussian process. This class of stochastic processes can be used to represent uncertain environmental excitations in structural engineering applications; see, e.g., [5, 38, 39, 40, 41, 42]. By applying the Karhunen-Loève expansion [43, 44], the discrete Gaussian load can be represented as

$$p(t_k,\boldsymbol{\theta}) = \mu_k + \boldsymbol{\psi}_k^T\boldsymbol{\theta},\ k = 1,\ldots,n_T \tag{3}$$

where $p(t_k,\boldsymbol{\theta})$ is the loading at time $t_k = (k-1)\Delta t, k = 1,\ldots,n_T$, Δt is the time step, $n_T = T/\Delta t + 1$ is the number of time instants; $\boldsymbol{\theta}$ is a realization of a standard Gaussian random variable vector of dimension n_θ; μ_k is the expected value of the stochastic process p at time t_k; and $\boldsymbol{\psi}_k$ is a vector of dimension n_θ associated with time instant t_k. The set of vectors $\boldsymbol{\Psi} = [\boldsymbol{\psi}_1,\ldots,\boldsymbol{\psi}_{n_T}]$ is given by $\boldsymbol{\Psi} = \boldsymbol{\Lambda}^{1/2}\boldsymbol{\Xi}^T$, where $\boldsymbol{\Lambda}$ and $\boldsymbol{\Xi}$ comprise, respectively, the n_θ largest eigenvalues and corresponding eigenvectors of the covariance matrix $\boldsymbol{\Sigma}$ of the stochastic load, i.e., $\boldsymbol{\Sigma}\boldsymbol{\Xi} = \boldsymbol{\Xi}\boldsymbol{\Lambda}$. Without loss of generality, a zero-mean stochastic process is assumed as $\mu_k = 0, k = 1,\ldots,n_T$. Finally, it is noted that the characterization of the stochastic load by means of Eq. (3) generally involves a large number of basic random variables, i.e., n_θ is usually in the order of hundreds or thousands [33].

2.3. Reliability constraints

Requirements on system reliability are usually established using failure probability measures. In this contribution, the reliability constraints are expressed in the form

$$r_j(\mathbf{x}) = \ln\left(P_{F_j}(\mathbf{x})\right) - \ln(P_{F_j}^*) \leq 0, \quad j = 1,\ldots,n_r \tag{4}$$

where $\ln(\cdot)$ denotes natural logarithm, $P_{F_j}(\mathbf{x})$ is the probability of failure event F_j evaluated at design $\mathbf{x}$, and $P^*_{F_j}$ is the corresponding maximum allowable value. In the context of structural dynamical systems under stochastic excitation, the probability that certain requirements are not fulfilled within the load duration T is a useful measure of structural performance. Thus, reliability requirements are expressed by means of *first-passage failure events* [45, 46]

$$F_j = \{d_j(\mathbf{x}, \boldsymbol{\theta}) > 1\}, \quad j = 1, \ldots, n_r \tag{5}$$

where $d_j(\mathbf{x}, \boldsymbol{\theta})$ is the *normalized demand function* of event F_j given by

$$d_j(\mathbf{x}, \boldsymbol{\theta}) = \max_{t\in[0,T]} \max_{m=1,\ldots,n_{j,h}} \frac{|h_{j,m}(t, \mathbf{x}, \boldsymbol{\theta})|}{h^*_{j,m}} \tag{6}$$

where $h_{j,m}(t, \mathbf{x}, \boldsymbol{\theta}), m = 1, \ldots, n_{j,h}$ are the response functions of interest associated with failure event F_j with corresponding threshold levels $h^*_{j,m} > 0$. The response functions are taken as linear combinations of the structural displacements, velocities and/or accelerations. As a result, they are time-dependent and also depend on the design and random variables. Finally, the *first-passage failure probability* associated with the j^{th} reliability constraint is given by

$$P_{F_j}(\mathbf{x}) = \int_{\boldsymbol{\theta}\in\mathbb{R}^{n_\theta}} I_{F_j}(\mathbf{x}, \boldsymbol{\theta}) f_{\boldsymbol{\Theta}}(\boldsymbol{\theta}) d\boldsymbol{\theta} \tag{7}$$

where $I_{F_j}(\mathbf{x}, \boldsymbol{\theta})$ is the indicator function with $I_{F_j}(\mathbf{x}, \boldsymbol{\theta}) = 1$ if $d_j(\mathbf{x}, \boldsymbol{\theta}) > 1$ and $I_{F_j}(\mathbf{x}, \boldsymbol{\theta}) = 0$ otherwise, and $f_{\boldsymbol{\Theta}}(\boldsymbol{\theta})$ is the standard multivariate Gaussian probability density function of dimension n_θ. As already pointed out, $\boldsymbol{\theta}$ may comprise hundreds or thousands of random variables. Therefore, the evaluation of the integral in Eq. (7) at each design represents a high-dimensional problem which is extremely demanding from the numerical viewpoint [45, 46]. As already pointed out, DIS [32, 34] is implemented to evaluate the reliability constraints and their first-order derivatives.

2.4. Optimum design sensitivity

The formulation of a RBO problem depends a number of parameters to characterize the objective and constraint functions and, therefore, changes in these quantities can affect the final solution [47]. Of particular importance are those involved in the definition of reliability constraints, e.g., excitation model parameters or response thresholds. For a given model parameter, ζ, the rates of change of the optimum objective value, $\frac{df^*}{d\zeta}$, and of the optimum values for the design variables,

$\frac{\partial x_i^*}{\partial \zeta}$, $i = 1, \ldots, n_x$, represent suitable sensitivity measures. These derivatives are associated with the greatest feasible improvement of the final solution for small changes in ζ. A direction-finding approach [37] is adopted in this contribution to compute such sensitivities.

3. Directional Importance Sampling

Directional Importance Sampling is a stochastic simulation method tailored to linear structural systems subject to Gaussian excitation [32, 34]. Consider a first-passage failure event $F = \{d(\boldsymbol{\theta}) > 1\}$ with normalized demand function $d(\boldsymbol{\theta}) = \max_{k=1,\ldots,n_T} \max_{m=1,\ldots,n_h} |h_m(t_k, \boldsymbol{\theta})|/h_m^*$. For notation simplicity, the explicit dependence of the different quantities on $\mathbf{x}$ has been dropped. Given the system linearity, the m^{th} response of interest evaluated at time t_k can be written as [48]

$$h_m(t_k, \boldsymbol{\theta}) = \mathbf{a}_{m,k}^T \boldsymbol{\theta}, \quad \mathbf{a}_{m,k} = \sum_{q=1}^{k} \epsilon_q \Delta t \eta_m(t_k - t_q) \boldsymbol{\psi}_q \tag{8}$$

where ϵ_q depends on the time integration rule [49] and $\eta_m(t)$ is the unit impulse response function computed using modal superposition.

The fundamental ideas of DIS can be summarized as follows. First, the concept of *directional sampling* [50, 51, 52] is considered. Instead of using full Cartesian coordinates, the reliability problem is expressed in terms of unit directions $\mathbf{u} \sim f_{\mathbf{U}}(\mathbf{u})$ uniformly distributed over the unit hypersphere $\Omega_{\mathbf{U}} \subset \mathbb{R}^{n_\theta}$. Second, an importance sampling density $f_{\mathbf{U}}^{\text{DIS}}(\mathbf{u})$ is introduced for the unit directions following some of the ideas presented in [29]. Third, the linearity of the responses of interest is exploited to obtain closed-form solutions for the probability of failure conditioned on each sampled direction. As a result, the failure probability can be written as

$$P_F = \int_{\Omega_{\mathbf{u}}} \left[1 - F_{\chi^2}^{n_\theta}\left(c(\mathbf{u})^2\right)\right] \left(\frac{f_{\mathbf{U}}(\mathbf{u})}{f_{\mathbf{U}}^{\text{DIS}}(\mathbf{u})}\right) f_{\mathbf{U}}^{\text{DIS}}(\mathbf{u}) d\mathbf{u} \tag{9}$$

where $F_{\chi^2}^{n_\theta}(\cdot)$ is the cumulative distribution function of the Chi-square distribution of n_θ degrees of freedom, and

$$c(\mathbf{u}) = \min_{\substack{m=1,\ldots,n_h \\ k=1,\ldots,n_T}} c_{m,k}(\mathbf{u}) = \min_{\substack{m=1,\ldots,n_h \\ k=1,\ldots,n_T}} \frac{h_m^*}{|\mathbf{a}_{m,k}^T \mathbf{u}|} \tag{10}$$

represents the minimum capacity-to-demand ratio across all responses of interest and time instants for the fixed unit vector $\mathbf{u}$. Equivalently, this quantity can be interpreted as the minimum factor by which $\mathbf{u}$ must be amplified to generate failure. Finally, a failure probability estimate is obtained by drawing samples $\mathbf{u}^{(\ell)} \sim f_{\mathbf{U}}^{\mathrm{DIS}}(\mathbf{u})$, $\ell = 1, \ldots, N$, which gives

$$P_F \approx \tilde{P}_F^{\mathrm{DIS}} = \frac{1}{N} \sum_{\ell=1}^{N} \frac{\hat{P}_F \left[1 - F_{\chi^2}^{n_\theta}\left(c(\mathbf{u}^{(\ell)})^2\right)\right]}{\sum_{m=1}^{n_h} \sum_{k=1}^{n_T} \left[1 - F_{\chi^2}^{n_\theta}\left(c_{m,k}(\mathbf{u}^{(\ell)})^2\right)\right]} \tag{11}$$

where $\hat{P}_F = 2\sum_{m=1}^{n_h}\sum_{k=1}^{n_T} \Phi(-h_m^*/\|\mathbf{a}_{m,k}\|)$ with $\Phi(\cdot)$ the standard Gaussian cumulative distribution function. In general, relatively small sample sizes are required to obtain sufficiently accurate reliability estimates [32]. Further, the sample generation process is highly efficient and parallelizable [30]. A detailed description of DIS can be found in [32].

4. Reliability sensitivity assessment framework

4.1. First-order derivatives with respect to general model parameters

Consider a general model parameter, ν, involved in the definition of the normalized demand function such that $F = \{d(\nu, \boldsymbol{\theta}) > 1\}$. Note that ν can affect the structural properties, the excitation model, or the response thresholds. Following the ideas presented in [34], direct differentiation of the integral in Eq. (9) with respect to ν yields

$$\frac{\partial P_F}{\partial \nu} = -\int_{\Omega_{\mathbf{U}}} \left[2c(\nu,\mathbf{u})\frac{\partial c(\nu,\mathbf{u})}{\partial \nu} f_{\chi^2}^{n_\theta}\left(c(\nu,\mathbf{u})^2\right)\right]\left(\frac{f_{\mathbf{U}}(\mathbf{u})}{f_{\mathbf{U}}^{\mathrm{DIS}}(\mathbf{u})}\right) f_{\mathbf{U}}^{\mathrm{DIS}}(\mathbf{u})d\mathbf{u} \tag{12}$$

where $f_{\chi^2}^{n_\theta}$ is the probability density function of the Chi-squared distribution of n_θ degrees of freedom. Then, the same set of samples generated to evaluate Eq. (11) can be used to estimate the first-order derivatives as

$$\frac{\partial P_F}{\partial \nu} \approx \frac{\partial \tilde{P}_F^{\mathrm{DIS}}}{\partial \nu} = -\frac{1}{N}\sum_{\ell=1}^{N} \frac{2\hat{P}_F(\nu)c(\nu,\mathbf{u}^{(\ell)})\frac{\partial c(\nu,\mathbf{u}^{(\ell)})}{\partial \nu} f_{\chi^2}^{n_\theta}\left(c(\nu,\mathbf{u}^{(\ell)})^2\right)}{\sum_{m=1}^{n_h}\sum_{k=1}^{n_T}\left[1 - F_{\chi^2}^{n_\theta}\left(c_{m,k}(\nu,\mathbf{u}^{(\ell)})^2\right)\right]} \tag{13}$$

In the previous equation, the only additional terms that need to be computed are $\frac{\partial c(\nu,\mathbf{u}^{(\ell)})}{\partial \nu}$, $\ell = 1, \ldots, N$. To this end, assume that $c(\nu,\mathbf{u}) = c_{M,K}(\nu,\mathbf{u})$, where (M, K) are the indices that provide the minimum in Eq. (10). Then, the sought partial derivative is

$$\frac{\partial c(\nu,\mathbf{u})}{\partial \nu} = \frac{\partial c_{M,K}(\nu,\mathbf{u})}{\partial \nu} = \frac{\partial}{\partial \nu}\left(\frac{h_M^*}{|\mathbf{a}_{M,K}^T\mathbf{u}|}\right) \tag{14}$$

Three different scenarios in terms of the type of model parameter can be identified. First, if ν affects structural properties, then the evaluation of Eq. (14) simply requires the sensitivities of the spectral properties [53]. Second, when ν represents an excitation model parameter, the derivatives of the vectors associated with the Karhunen-Loève expansion (see Eq. (3)) are needed. This can be carried out using any suitable method [54]. Finally, in case ν corresponds to a response threshold, sensitivity evaluation can be performed with marginal computational efforts. For completeness, Appendix A provides explicit formulas for the three different scenarios in terms of ν.

4.2. Practical advantages

From the practical viewpoint, the adopted reliability sensitivity assessment framework presents two main advantageous features. On the one hand, the formulation presented in this section is quite general in the sense that it can be used to estimate sensitivities with respect to both design variables ($\nu = x_i$) and alternative model parameters ($\nu = \zeta$). On the other hand, the comparison of Eqs. (11) and (13) reveals that all the information retrieved during reliability assessment is reused to compute the corresponding first-order derivatives. Thus, first-order derivatives of reliability measures can be obtained as a byproduct of reliability assessment. These features are quite beneficial in the context of RBO problems, as they enable effective gradient-based solution schemes to obtain optimum solutions and to evaluate the sensitivity of final designs.

5. Implementation of first-order solution methods

5.1. Sequential optimization strategy

In order to solve the RBO problem in Eq. (1), a first-order sequential optimization approach based on a class of feasible-direction interior point algorithms [35, 36] is adopted. In essence, each optimization cycle requires to identify a feasible-descent direction and to solve a line search problem to find a new candidate along such direction. Several advantages are provided by the adopted optimization strategy. First, the method produces a sequence of feasible designs with consecutively lower objective function values. Hence, the optimization process can be stopped at any iteration to retrieve a feasible solution that is better than the initial one. Second, one-dimensional surrogates for the reliability constraints, instead of multi-dimensional surrogates, can be adaptively generated during each optimization cycle for improved computational efficiency. Finally, relatively few reliability analyses are usually required to reach convergence. The reader is referred to [35] for a detailed description of the optimization strategy.

5.2. Direction-finding approach for optimum design sensitivity

In this contribution, the framework proposed in [37] is adopted to compute optimum design sensitivities. Consider the augmented design space $\langle x_1, \ldots, x_{n_x}, \zeta \rangle$ of dimension $n_x + 1$, where ζ represents a given model parameter. Then, sensitivity computation can be viewed as finding the *constrained steepest-descent direction* in such augmented space, $\mathbf{s} = [s_1, \ldots, s_{n_x+1}]^T$, which provides the greatest improvement of the objective value while satisfying the problem constraints. This direction is the solution to [37, 55]

$$\begin{aligned} \min_{\mathbf{s}} \quad & \nabla f^T \mathbf{s} \\ \text{s.t.} \quad & \nabla r_j^T \mathbf{s} \leq 0, \qquad j \in J_r \\ & \nabla g_j^T \mathbf{s} \leq 0, \qquad j \in J_g \\ & \mathbf{s}^T \mathbf{s} - 1 \leq 0 \end{aligned} \tag{15}$$

where $\nabla \mathcal{F}^T = \left[\frac{\partial \mathcal{F}(\mathbf{x},\zeta)}{\partial x_1}, \ldots, \frac{\partial \mathcal{F}(\mathbf{x},\zeta)}{\partial x_{n_x}}, \frac{\partial \mathcal{F}(\mathbf{x},\zeta)}{\partial \zeta} \right] \Big|_{\mathbf{x}^*, \zeta^0}$, with $\mathcal{F}$ representing f, r_j, $j \in J_r$, or g_j, $j \in J_g$; ζ^0 is the nominal or actual value of ζ; and J_r and J_g denote the sets of reliability and standard constraints, respectively, that are active at the final design $\mathbf{x}^*$. It is seen that the framework only requires the first-order derivatives of the objective and active constraint functions with respect to x_i, $i = 1, \ldots, n_x$, and ζ. Furthermore, the previous optimization problem can be solved very efficiently, as it involves a linear objective function, linear constraints and a single quadratic constraint [56]. Based on the direction $\mathbf{s}$, the rate of change of the optimum objective is [37]

$$\frac{df^*}{d\zeta} = \frac{\nabla f(\mathbf{x}^*, \zeta^0)^T \mathbf{s}}{|s_{n_x+1}|} \tag{16}$$

and the rates of change of the optimum values for the design variables are computed as [37]

$$\frac{\partial x_i^*}{\partial \zeta} = \frac{s_i}{|s_{n_x+1}|}, \; i = 1, \ldots, n_x \tag{17}$$

If s_{n_x+1} is positive (negative), the previous results are associated with an increase (decrease) in ζ. In case $s_{n_x+1} = 0$, the optimum solution remains unaffected by changes in ζ. If the sign of the change in ζ is specified beforehand, a similar technique can be adopted [37].

Note that all the derivatives of the problem functions with respect to the design variables are readily available from the final optimization cycle. Therefore, only the sensitivities with respect to ζ remain to be evaluated, which is performed by reusing the DIS results at the final design. In other words, optimum design sensitivities are obtained as an effective post-process of the optimization results, which is advantageous for practical purposes.

5.3. Remarks

As already pointed out, DIS provides efficient estimation of failure probabilities and their sensitivities for linear structural systems subject to Gaussian excitation. This, in turn, enables first-order solution methods for RBO and optimum design sensitivity analysis. The specific strategies adopted in this work have proved quite effective, as illustrated in Section 6. Nonetheless, the use of DIS in RBO problems is not necessarily limited to these particular solution methods. In principle, any suitable method that requires only the gradients of failure probability functions can be integrated with the sensitivity analysis framework described in this contribution. Hence, DIS can be interpreted as a potentially useful and numerically efficient tool to aid informed decision-making processes under uncertainty. Furthermore, this suggests that exploiting particular features of specialized simulation techniques can be quite advantageous for RBO schemes.

6. Example problem

In order to illustrate the applicability of the proposed framework, a numerical example involving a realistic building model subject to stochastic loading is presented in this section. The goal of this example is to determine the thicknesses of the core shear walls that minimize structural weight, subject to constraints on serviceability reliability and geometric conditions. Two scenarios in terms of the number of design variables and the number of reliability constraints are addressed. In addition, the sensitivity of the optimum design with respect to response thresholds and excitation model parameters is studied.

6.1. Building structure

A three-dimensional finite element model of a 16-story reinforced concrete (RC) building, which has been borrowed from [34], is considered in this section. For illustration purposes, Fig. 1 shows a three-dimensional representation of the structural model. The interstory height is equal to 3.25 m, which gives a total height of 52.0 m. In addition, the building is 30 m by 35 m in plan. A perimeter of RC rectangular columns and shear walls plus a core of RC shear walls are considered for the horizontal resistant system. The corresponding material properties are given by Young modulus $E = 2.5 \times 10^{10}$ N/m^2, Poisson ratio equal to 0.3, and mass density equal to 2500 kg/m^3.

Shell elements of different thicknesses are considered to model the shear walls and floor slabs. In addition, beam and column elements are also included in the system. As a result, the finite element model involves 29466 degrees of freedom. Since the system is studied for small vibrations, linear elastic behavior is assumed. Finally, 20 modes are kept for dynamic analysis purposes and a 5% of critical damping is considered for all modes.

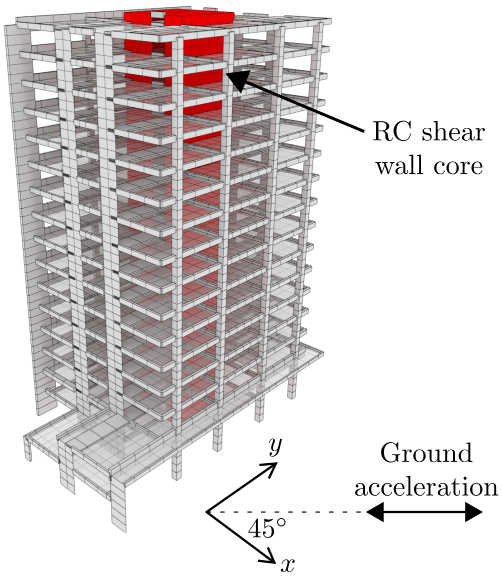

Figure 1: Perspective view of a 16-story reinforced concrete structure under ground excitation.

6.2. Stochastic ground excitation

As illustrated in Fig. 1, the building is subject to a ground excitation applied at 45° with respect to the x axis. Such loading is modeled as a non-stationary filtered white noise process with duration $T = 10$ s and time step $\Delta t = 0.01$ s. Specifically, a modulated white noise signal passing through a Clough-Penzien filter [57] is considered. Hence, the ground acceleration is given by $\ddot{u}_g(t) = \Omega_1^2 w_1(t) + 2\xi_1\Omega_1\dot{w}_1(t) - \Omega_2^2 w_2(t) - 2\xi_2\Omega_2\dot{w}_2(t)$, where $\Omega_1 = 15.6$ rad/s, $\Omega_2 = 1.0$ rad/s, $\xi_1 = 0.6$ and $\xi_2 = 0.9$ are the filter parameters, and the variables $w_i(t)$, $i = 1, 2$, satisfy the set of coupled differential equations

$$\begin{aligned} \ddot{w}_1(t) + 2\xi_1\Omega_1\dot{w}_1(t) + \Omega_1^2 w_1(t) &= w(t)h(t) \\ \ddot{w}_2(t) + 2\xi_2\Omega_2\dot{w}_2(t) + \Omega_2^2 w_2(t) &= \Omega_1^2 w_1(t) + 2\xi_1\Omega_1\dot{w}_1(t) \end{aligned} \tag{18}$$

where $w(t)$ is a white noise process with spectral intensity $S = 1.5 \times 10^{-3}$ m^2/s^3, and $h(t)$ is a time envelope function defined as

$$h(t) = \begin{cases} (t/5)^2 & 0 \leq t \leq 5 \text{ s} \\ 1 & 5 < t \leq 6 \text{ s} \\ e^{-(t-6)^2} & t > 6 \text{ s} \end{cases} \tag{19}$$

Finally, for illustration purposes, all the eigenvalues of the covariance matrix of the stochastic process are retained to construct the Karhunen-Lòeve expansion and, as a result, the number of basic random variables is given by $n_\theta = n_T = 1001$. Therefore, the discrete representation of the stochastic ground acceleration involves a large number of basic random variables for this case.

6.3. Scenario I: Design problem

For illustration purposes, $n_x = 2$ design variables and a single reliability constraint are considered in this scenario. The thicknesses of the core shear walls of the eight lower stories are linked to the first design variable as $t_{w,s} = \bar{t}_w x_1$, $s = 1, \ldots, 8$, whereas that of the remaining stories is linked to the second design variable as $t_{w,s} = \bar{t}_w x_2$, $s = 9, \ldots, 16$, with $\bar{t}_w = 0.4$ m the reference thickness value. The constrained RBO problem is given by

$$\begin{aligned} \min_{\mathbf{x}=[x_1,x_2]^T} \quad & f(\mathbf{x}) = (x_1 + x_2)/2 \\ \text{s.t.} \quad & r(\mathbf{x}) = \ln(P_F(\mathbf{x})) - \ln(10^{-3}) \leq 0 \\ & g(\mathbf{x}) = x_2 - x_1 \leq 0 \\ & 0.5 \leq x_i \leq 2.0, \quad i = 1, 2 \end{aligned} \tag{20}$$

where $f(\mathbf{x})$ is associated with the weight of the core shear walls, $P_F(\mathbf{x})$ is a failure probability function with maximum allowable value $P_F^* = 10^{-3}$, and $g(\mathbf{x}) \geq 0$ is a geometric constraint. Note that this formulation imposes $x_2 \leq x_1$, i.e., walls of lower floors must be thicker than of upper floors. This is a usual consideration in the context of structural design procedures. In addition, the constraints $0.5 \leq x_i \leq 2.0$, $i = 1, 2$, indicate that the core wall thicknesses lie between 0.2 m and 0.8 m. The failure event F is associated with serviceability conditions, and it is defined as

$$F = \left\{ \max_{m=1,\ldots,16} \max_{k=1,\ldots,1001} \left(\frac{|h_{m,x}(t_k, \mathbf{x}, \boldsymbol{\theta})|}{h_m^*}, \frac{|h_{m,y}(t_k, \mathbf{x}, \boldsymbol{\theta})|}{h_m^*} \right) > 1 \right\} \tag{21}$$

where $h_{m,x}(t_k, \mathbf{x}, \boldsymbol{\theta})$ and $h_{m,y}(t_k, \mathbf{x}, \boldsymbol{\theta})$ are the interstory drifts, expressed as a percentage of the floor height, between floors m and $m-1$ along the x and y directions, respectively, and $h_m^* = 0.1\%$, $m = 1, \ldots, 16$, represent the corresponding maximum allowable values. It is assumed that $m = 0$

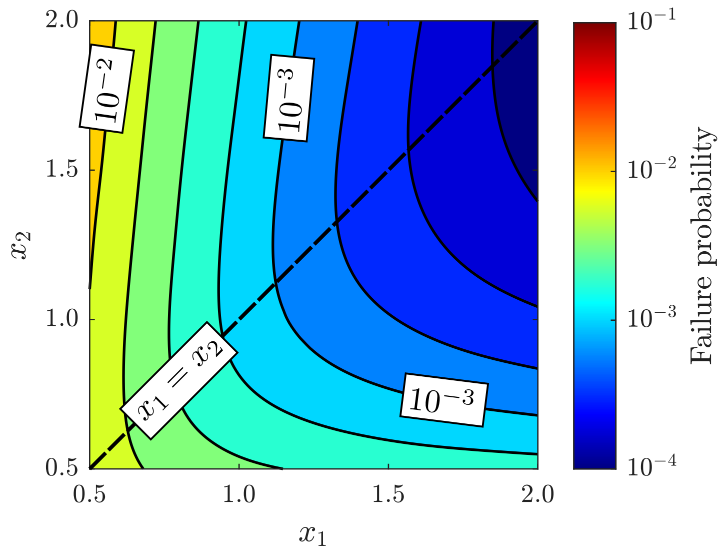

Figure 2: Contours of the failure probability function $P_F(\mathbf{x})$. Scenario I.

represents the ground floor. In this setting, failure is defined when any interstory drift along the x or y axes exceeds 0.1% of its corresponding floor height. Such failure criterion can be related, for instance, to the violation of a serviceability limit state of the RC core walls [58]. Finally, it is noted that the evaluation of the failure probability at any given design, $P_F(\mathbf{x})$, represents a challenging problem as it involves a high-dimensional integration domain, a finite element model with thousands of degrees of freedom, and more than 30000 elementary failure domains.

To obtain insight about the design problem, Fig. 2 shows the contours of $P_F(\mathbf{x})$. These iso-probability curves have been obtained by considering a set of DIS-based failure probability estimates distributed over the design space. The resulting curves, which are somewhat rugged due to the inherent variability of the estimates, have been smoothed for presentation purposes. From the figure, it is seen that the failure probability seems to be minimized by increasing the core wall thicknesses as much as possible, as expected. In general, the failure probability function depends mainly on x_1 when $x_2 > x_1$, i.e., when the upper core walls are thicker than the lower ones. Meanwhile, a stronger interaction between x_1 and x_2 is observed for $x_2 < x_1$. In this case, an increase in the thickness of the lower core walls can be compensated by a decrease in the thickness of the upper walls to maintain the same reliability level. These results are reasonable from a structural viewpoint. For comparison and reference purposes, Fig. 3 shows a sketch of the feasible design set. Some contours of the objective function and a reference location for the optimum design are also presented in the figure. Note that only the reliability constraint is active at the optimum solution.

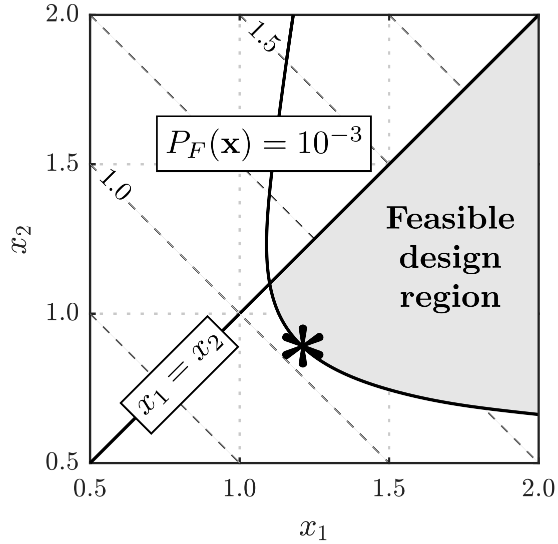

Figure 3: Sketch of the feasible design space, objective contours and optimum design ($*$). Scenario I.

6.4. Scenario I: Results

6.4.1. Reliability sensitivity estimates

First-order information on the problem functions is used by the adopted optimization strategy to explore the design space efficiently. Typically, candidate design trajectories tend to move along boundaries of the feasible design set until reaching the optimum region [36]. In this context, poor quality information about the sensitivity of the active constraints can lead to spurious behavior of the optimization process, since identified search directions might not be actually feasible. Therefore, it is particularly important for the convergence of the algorithm to obtain sufficiently accurate estimates of the gradients of the active reliability constraint functions. For this example, the gradient of the reliability constraint function in Eq. (20) is estimated as $\frac{\partial r(\mathbf{x})}{\partial x_i} \approx \frac{1}{\tilde{P}_F^{\mathrm{DIS}}(\mathbf{x})} \frac{\partial \tilde{P}_F^{\mathrm{DIS}}(\mathbf{x})}{\partial x_i}$, $i = 1, 2$. In this regard, the choice of an inadequately small sample size can affect the optimization procedure as such sensitivity estimates might have an unacceptable level of variability. Validation calculations have shown that $N = 2000$ samples provide a reasonable tradeoff between computational cost and quality of the DIS results in this example. For illustration purposes, Fig. 4 presents the estimates of $\nabla r(\mathbf{x})$ obtained across 20 independent DIS runs with $N = 2000$ samples. These estimates are evaluated at the design $\mathbf{x} = [1.18, 0.93]^T$, which verifies $P_F(\mathbf{x}) \approx 10^{-3}$. It is seen that the gradient estimates point in a similar direction and, overall, their quality is acceptable in the context of RBO problems involving structural dynamical systems under stochastic excitation.

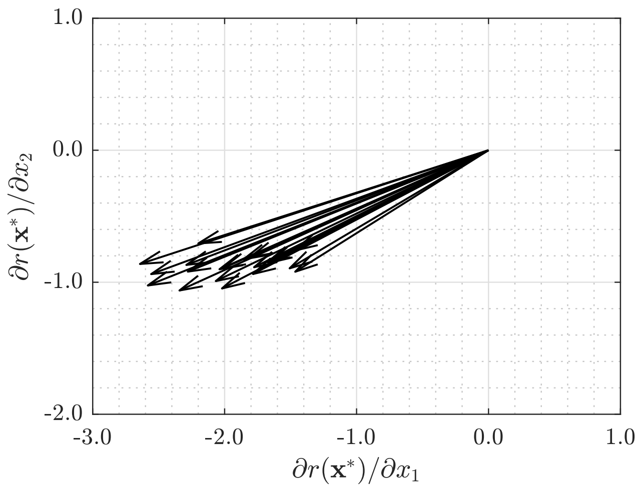

Figure 4: Estimates of the reliability constraint gradient obtained in 20 independent DIS runs. Scenario I.

6.4.2. *Optimization process*

The sequential optimization strategy presented in Section 5.1 is implemented to solve problem (20). As already pointed out, this optimization strategy uses sensitivity information provided by DIS to produce a sequence of feasible designs with decreasing objective function values. The recommendations provided in [35, 36] are considered for numerical implementation. Additionally, a sample size equal to $N = 2000$ is considered for DIS. Furthermore, the customary technique of using common random number streams is implemented, which means that the same sequence of pseudorandom numbers is considered for reliability assessment at each design. Numerical experience indicates that this strategy is quite effective in reducing the effect of the variability of the estimators on RBO procedures [59]. Three different cases in terms of the starting point are studied to evaluate the performance of the optimization scheme. In particular, cases A, B and C correspond to initial designs $\mathbf{x}^{\mathrm{A}} = [1.95, 1.90]^T$, $\mathbf{x}^{\mathrm{B}} = [1.95, 0.80]^T$ and $\mathbf{x}^{\mathrm{C}} = [1.75, 1.00]^T$, respectively. It is noted that the method requires an initial design that is feasible, which can be usually identified using engineering judgment. However, in involved cases where a feasible design is difficult to identify a priori, systematic methods can be implemented to find a starting point [47].

The sequences of candidate designs obtained for the three different starting points under consideration are presented in Fig. 5, where the corresponding final solutions are highlighted using dark markers. For reference purposes, some contours of the objective function $f(\mathbf{x})$ are also shown in the figure. In general, the method reaches the active feasible boundary in few optimization cycles. Then, candidate solutions tend to move along that boundary, which in this case is associated with the reliability constraint. Additionally, the three final designs are very similar between each other and they seem to lie along a contour of $f(\mathbf{x})$. To obtain further insight about the optimization process, the objective function values obtained during the different optimization cycles are presented in Fig. 6. Note that eight iterations are required in all cases to verify the stopping criterion. From the figure, it is clear that significant improvements in the objective function values are obtained during the initial algorithm iterations, which is beneficial for the type of problems under consideration. In case A, for instance, a relative improvement of approximately 45% is attained after the four initial optimization cycles for case. This behavior is consistent with the large initial displacements in the search space observed in Fig. 5. Finally, Table 1 presents the optimum designs obtained by the optimization scheme for the three different starting points. For comparison purposes, a reference solution obtained from a direct double-loop implementation is also presented in the table. This design has been obtained using direct Monte Carlo simulation and genetic algorithms [59] with a population size of 50 individuals. Very similar objective function values are observed for all cases. In fact, the maximum relative difference between the objective values of all the reported solutions is less than 0.5%. Thus, the integration of DIS and suitable gradient-based methods provides optimum designs in an effective manner. Finally, the reliability constraint can be regarded as active while the geometric constraint remains inactive for all the designs reported in the table, as expected.

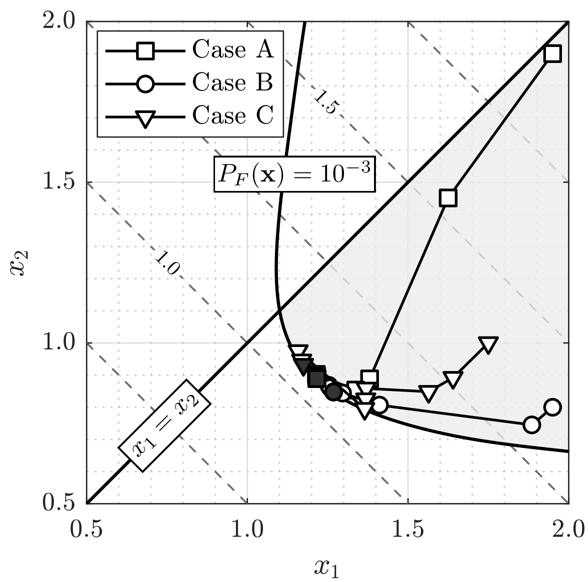

Figure 5: Trajectories of candidate designs corresponding to three different starting points. Scenario I.

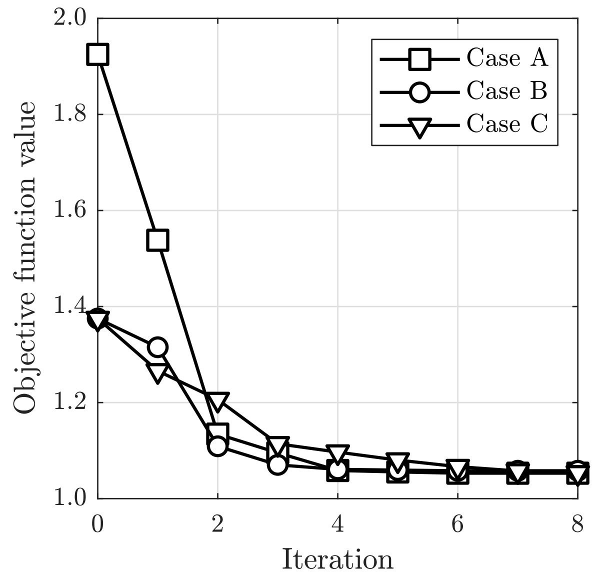

Figure 6: Evolution of candidate objective function values for three different starting points. Scenario I.

	Case A	Case B	Case C	Reference
x_1^*	1.217	1.268	1.175	1.177
x_2^*	0.889	0.848	0.932	0.928
$P_F(\mathbf{x}^*)/10^{-3}$	0.999	0.999	0.995	0.999
$g(\mathbf{x}^*)$	-0.327	-0.421	-0.242	-0.249
$f(\mathbf{x}^*)$	1.0529	1.0580	1.0536	1.0525

Table 1: Final designs corresponding to three different starting points and reference solution. Scenario I.

6.4.3. Comparison with a finite difference implementation

As discussed in Section 4, the sensitivity assessment framework enabled by DIS provides first-order derivatives by post-processing the sampling results. In principle, an alternative means of computing such derivatives is to use finite differences and DIS. To compare the performance of both sensitivity assessment methods, they are integrated with the optimization strategy presented in Section 5.1 to solve the RBO problem in Eq. (20). Central differences are considered and, therefore, a total of five DIS estimates are required to evaluate the reliability constraint function and its gradient at each design. Validation calculations indicate that a total of $N = 2000$ samples are adequate for both sensitivity assessment techniques.

Table 2 summarizes the results obtained by both approaches in terms of the final design, number of optimization cycles (N_{cycles}), and total number of reliability analyses (N_{rel}). For conciseness, only case A is presented in the table. However, validation calculations indicate that similar results are obtained for alternative starting points. Several observations can be made from this table. First, both approaches provide very similar final designs in terms of the objective value. Second, the use of finite differences requires to define an appropriate perturbation step, whereas the framework described in Section 4 circumvents this need. This is an advantage from the practical viewpoint. Third, the proposed approach needs only eight optimization cycles (see Fig. 6) whereas the implementation with finite differences requires 12 iterations. Fourth, the number of reliability analyses required by the finite difference implementation is significantly higher than by the proposed approach. In fact, the proposed approach requires 35 reliability analyses, which are associated with the full evaluation of approximately four designs per optimization cycle. Meanwhile, the finite difference implementation requires a total of 640 DIS runs, which is roughly equivalent to the full evaluation of 10 designs per optimization cycle. This behavior can be attributed to the higher variability of sensitivity estimates obtained with finite differences, which tends to reduce the performance of gradient-based optimization methods. For this case, not only such variability affects the choice of the feasible-descent direction in each optimization cycle, but is also detrimental to the convergence of the subsequent line search procedure. Finally, the previous observations indicate that the computational burden of the proposed approach is significantly lower than of using finite differences and, in addition, it provides additional advantages for practical implementation purposes.

	Proposed approach	Finite differences
x_1^*	1.217	1.269
x_2^*	0.889	0.847
$P_F(\mathbf{x}^*)/10^{-3}$	0.999	0.998
$g(\mathbf{x}^*)$	-0.327	-0.422
$f(\mathbf{x}^*)$	1.0529	1.0580
N_{cycles}	8	12
N_{rel}	35	640

Table 2: Optimization results obtained with the proposed approach and an implementation based on finite differences. Case A. Scenario I.

6.4.4. Sensitivity of the optimum design with respect to response thresholds

Optimum design sensitivity assessment provides information on how optimum solutions can change under model parameter perturbations. As described in Section 5.2, this is achieved by integrating a direction-finding approach for optimum design sensitivity analysis with the general sensitivity assessment framework enabled by DIS. For illustration purposes and to show the type of results that can be obtained by the proposed scheme, the sensitivities of the optimum design with respect to the different response thresholds are considered here. Explicit formulas for the computation of these sensitivity measures can be found in Appendix A. Note that, in this case, reliability sensitivity assessment involves negligible computational efforts.

To evaluate the quality of the estimates obtained by the adopted framework, Fig. 7 shows the evolution, in terms of the number of samples, of the DIS-based estimates of $\frac{\partial P_F}{\partial h_s^*}$, $s = 7, 9, 10, 11$, evaluated at the final design of case A (see Table 1). The rest of the sensitivities are almost zero. From the figure, it is noted that all derivatives are negative. In other words, the failure probability tends to decrease when the maximum allowable values for the different interstory drifts are increased. This is reasonable from an engineering perspective, since higher threshold values correspond to more permissive performance requirements and, as a result, failure becomes less likely in such cases. In addition, it is noted that the estimates become rather stable for $N \geq 2000$ samples. Thus, obtaining first-order derivatives of the failure probability with respect to the response thresholds as a byproduct of the reliability assessment step at the final design, which involves $N = 2000$ samples, is adequate in the context of this example.

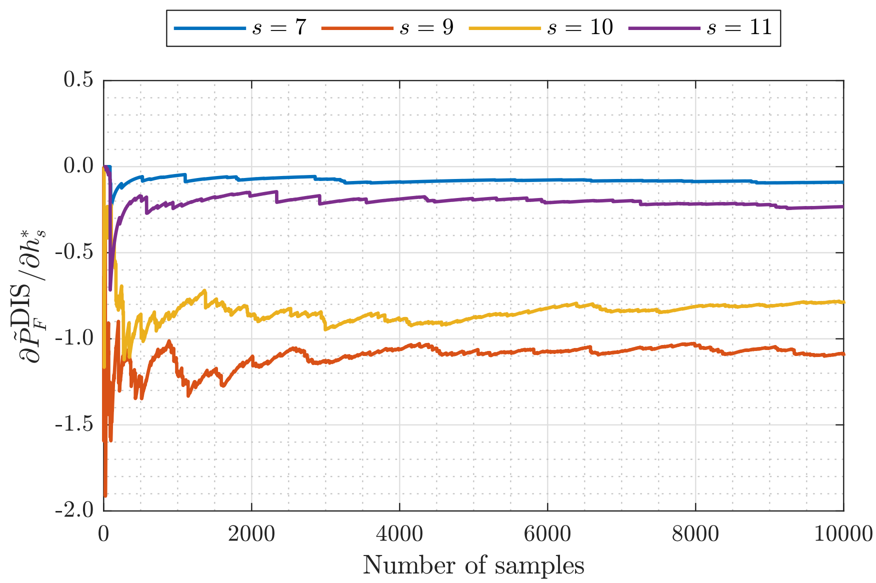

Figure 7: Evolution of the estimator of the partial derivative of the failure probability with respect to different response thresholds (h_s^*) in terms of the number of samples. Scenario I.

Once the first-order derivative of the reliability constraint with respect to each threshold h_s^* is obtained, the approach presented in Section 5.2 is implemented to obtain the sought optimum design sensitivity measures. Table 3 reports the results corresponding to the final design obtained in case A. However, validation calculations show that similar results are obtained for all final solutions reported in Table 1. For presentation purposes, all quantities in the table are normalized by a factor that ensures that the maximum absolute value of the optimum objective sensitivities is equal to one. Several observations can be made from these results. First, the final design is only sensitive to the response thresholds corresponding to stories 7, 9, 10 and 11, which are associated with the non-zero sensitivities reported in Fig. 7. Hence, perturbations of the maximum allowable drift values associated with lower and upper stories do not affect the optimum solution in this case. Second, all values presented in the table are negative, i.e., the greatest improvement in the optimum design is obtained by reducing the values of the design variables. Further, the solution of the direction-finding problem in Eq. (15) indicates that the results in the table correspond to increases of the different thresholds ($\delta h_s^* > 0$). Note that this behavior is reasonable from the engineering viewpoint since, as already pointed out, higher allowable values for the responses of interest lead to less restrictive design conditions. This highlights one of the advantages of the chosen method for optimum design sensitivity analysis, as it can identify the sign of the perturbation (increase or decrease) that is most beneficial toward improving the final solution. Third, the direction in which the optimum design tends to move is identical for all thresholds and is opposite to the objective function gradient. Fourth, the relative importance of the different parameters with respect to the final solution can be established from the optimum design sensitivity results. In this regard, Table 3 indicates that h_9^* and h_{10}^* are the most relevant parameters, h_7^* and h_{11}^* are less important, and the rest of thresholds do not affect the final design. Finally, the previous results illustrate that the implementation of DIS allows to obtain non-trivial information about final designs and their sensitivities.

Story (s)	df/dh_s^*	$\partial x_1^*/\partial h_s^*$	$\partial x_2^*/\partial h_s^*$
1–6	0	0	0
7	−0.12	−0.12	−0.12
8	0	0	0
9	−1.00	−1.00	−1.00
10	−0.91	−0.91	−0.91
11	−0.28	−0.28	−0.28
12–16	0	0	0

Table 3: Normalized sensitivities of the optimum objective value and of the optimum values for the design variables with respect to the maximum allowable interstory drifts. Scenario I.

6.5. Scenario II: Design problem

In this scenario, a more complex optimization problem in terms of the number of design variables and the number of constraints is studied. In particular, a total of $n_x = 8$ intermediate design variables are considered. Each design variable is linked to the thickness of the core walls of two consecutive floors as $t_{w,2i-1} = t_{w,2i} = \bar{t}_w x_i,\ i = 1, \ldots, 8$ (see Table 4). In addition, seven geometric constraints and 16 reliability constraints are imposed. The resulting optimization problem is stated as

$$\begin{aligned} \min_{\mathbf{x}} \quad & f(\mathbf{x}) = \textstyle\sum_{i=1}^{8} x_i \big/ 8 & \\ \text{s.t.} \quad & r_j(\mathbf{x}) = \ln(P_{F_j}(\mathbf{x})) - \ln(5 \times 10^{-4}) \leq 0, & j = 1, \ldots, 16 \\ & g_j(\mathbf{x}) = x_{j+1} - x_j \leq 0, & j = 1, \ldots, 7 \\ & 0.5 \leq x_i \leq 2.0, & i = 1, \ldots, 8 \end{aligned} \tag{22}$$

Design variable	x_1	x_2	x_3	x_4	x_5	x_6	x_7	x_8
Core walls (floors)	1–2	3–4	5–6	7–8	9–10	11–12	13–14	15–16

Table 4: Linking detail of intermediate design variables. Scenario II.

where the constraints $g_j(\mathbf{x}) \leq 0,\ j = 1, \ldots, 7$, ensure that walls of lower floors are thicker than of upper floors, and $P_{F_j}(\mathbf{x}),\ j = 1, \ldots, 16$ are failure probability functions with maximum value $P_F^* = 5 \times 10^{-4}$. Note that this value is smaller than the one considered in the previous scenario. The failure events are defined in terms of the normalized interstory drifts as

$$F_j = \left\{ \max_{k=1,\ldots,1001} \left(\frac{|h_{j,x}(t_k, \mathbf{x}, \boldsymbol{\theta})|}{h_j^*}, \frac{|h_{j,y}(t_k, \mathbf{x}, \boldsymbol{\theta})|}{h_j^*} \right) > 1 \right\} \tag{23}$$

with $h_j^* = 0.1\%$, $j = 1, \ldots, 16$. Hence, the j^{th} failure probability function is associated with the drift responses, along the x and y directions, of the j^{th} story.

6.6. Scenario II: Results

6.6.1. Optimization results

The sequential optimization strategy presented in Section 5.1 is implemented, and a total of $N = 3000$ samples are considered for reliability assessment. To illustrate the effectiveness of the optimization scheme in terms of the starting point, three different initial designs are considered, which are presented in Table 5.

	x_1	x_2	x_3	x_4	x_5	x_6	x_7	x_8
Case A	1.98	1.97	1.96	1.95	1.94	1.93	1.92	1.91
Case B	1.75	1.74	1.73	1.72	1.50	1.49	1.48	1.47
Case C	1.60	1.50	1.40	1.30	1.20	1.10	1.05	1.00

Table 5: Initial designs corresponding to different cases. Scenario II.

Figure 8 shows the candidate objective values obtained throughout the optimization process for the different starting points. From the figure, it is seen that cases A, B and C require 11, 14 and 12 optimization cycles, respectively, to verify the stopping criterion. However, in all cases it is possible to obtain a design that is very similar to the final solution after roughly 10 optimization cycles. This behavior is consistent with the results observed in the previous scenario, since the method is able to reduce significantly the objective values after few optimization cycles. Moreover, the final objective function values obtained in the different cases are very similar between each other. Regarding computational cost, it is noted that each optimization cycle requires the full reliability assessment of a number of designs associated with the identification of the step size along the search direction [36]. In this context, an average of three designs must be evaluated during each optimization cycle, leading to a total of less than 50 reliability analyses in all cases. This number is relatively small in the context of RBO problems. This highlights some of the benefits of adopting DIS as sensitivity assessment framework, since the use of gradient-based optimization strategies provides greatly improved designs with relatively few reliability analyses. Such a feature represents a significant advantage when compared, e.g., with stochastic search-based methods [22, 30].

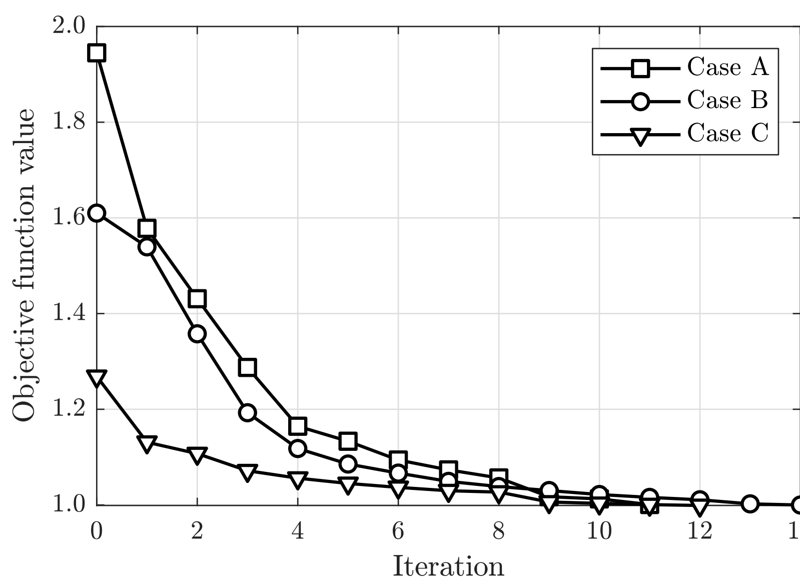

Figure 8: Evolution of candidate objective function values for three different initial designs. Scenario II.

Table 6 shows the final designs obtained for the three starting points under consideration. In addition, Table 7 reports the corresponding values of the active constraint functions that are regarded as active at the final designs. These correspond to the normalized failure probabilities $P_{F_j}(\mathbf{x})/P_F^*$, $j = 9, 10, 11$, with $P_F^* = 5 \times 10^{-4}$, and $g_j(\mathbf{x})$, $j = 2, 3, 4, 7$. The results indicate that all final designs are quite similar from the objective and constraint viewpoints. In fact, the maximum relative difference between the optimum objective values is about 0.2%. Thus, the first-order method enabled by DIS allows an effective exploration of the design space for this scenario. To gain further insight into the optimization process, Fig. 9 presents the evolution of the values of the constraint functions that are active at the final solution for case A. It is seen that the method requires about nine optimization cycles to reach a boundary of the feasible design set where all constraints under consideration are practically active. Such constraints tend to remain active during the rest of the optimization process. In other words, the search directions identified during the next iterations tend to follow such feasible boundary, which is consistent with the behavior observed in the previous scenario.

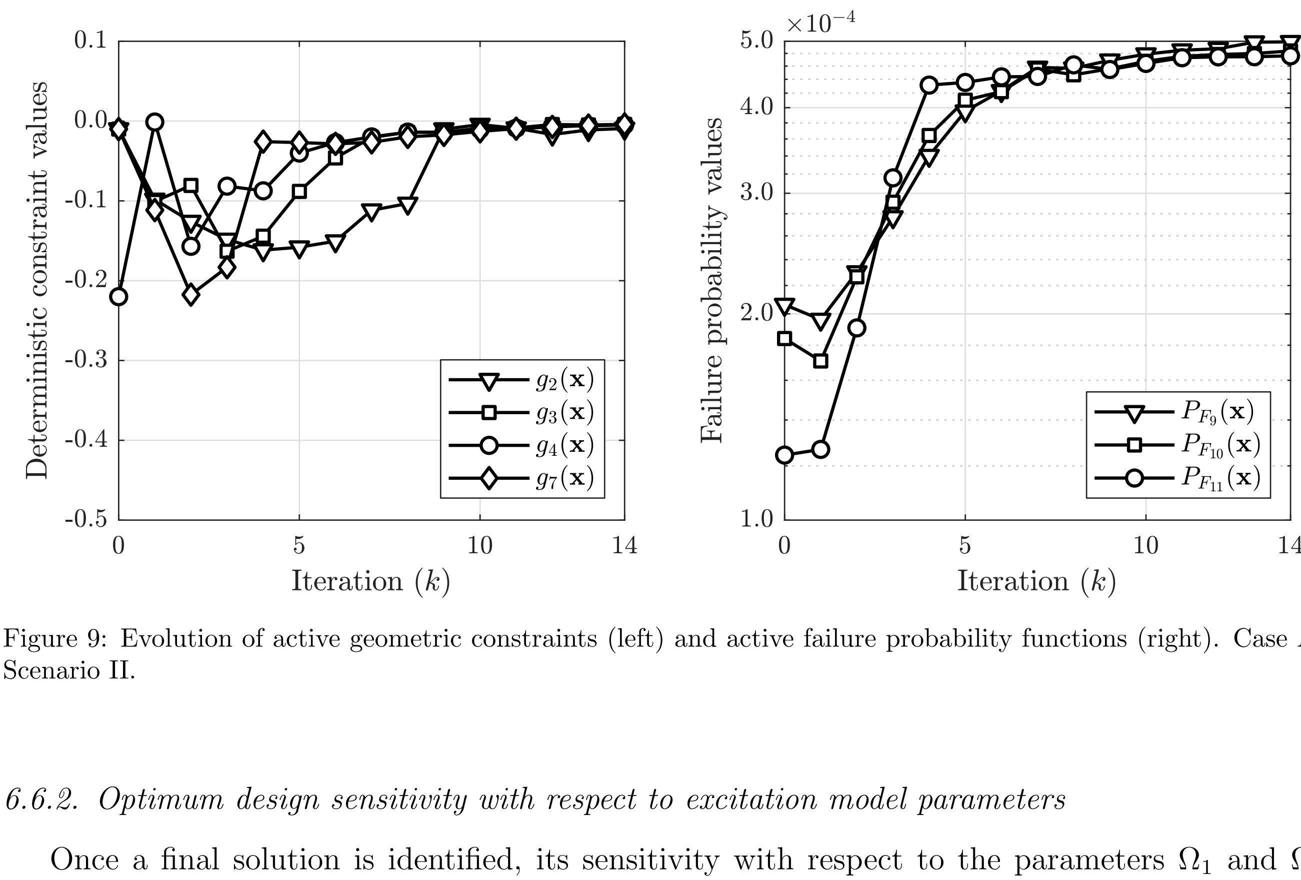

Figure 9: Evolution of active geometric constraints (left) and active failure probability functions (right). Case A. Scenario II.

6.6.2. *Optimum design sensitivity with respect to excitation model parameters*

Once a final solution is identified, its sensitivity with respect to the parameters Ω_1 and Ω_2 involved in the definition of the excitation model (see Section 6.2) is investigated. The approach described in Section 5.2 is implemented, which requires the first-order derivatives of the active

	Case A	Case B	Case C
x_1^*	1.528	1.500	1.498
x_2^*	1.141	1.141	1.141
x_3^*	1.126	1.132	1.130
x_4^*	1.122	1.128	1.129
x_5^*	1.118	1.123	1.125
x_6^*	0.962	0.961	0.959
x_7^*	0.507	0.509	0.507
x_8^*	0.504	0.505	0.504
$f(\mathbf{x}^*)$	1.001	0.999	0.999

Table 6: Final designs corresponding to three different starting points. Scenario II.

	Case A	Case B	Case C
$P_{F_9}(\mathbf{x}^*)/P_F^*$	0.994	0.998	0.995
$P_{F_{10}}(\mathbf{x}^*)/P_F^*$	0.968	0.968	0.968
$P_{F_{11}}(\mathbf{x}^*)/P_F^*$	0.953	0.952	0.961
$g_2(\mathbf{x}^*)$	-0.015	-0.009	-0.011
$g_3(\mathbf{x}^*)$	-0.004	-0.004	-0.001
$g_4(\mathbf{x}^*)$	-0.004	-0.005	-0.004
$g_7(\mathbf{x}^*)$	-0.003	-0.004	-0.003

Table 7: Active constraint functions corresponding to three different starting points. Scenario II.

reliability constraint functions with respect to these parameters. As previously pointed out, such quantities can be computed by post-processing the DIS results. In this context, since Ω_1 and Ω_2 affect the properties of the excitation model, the only additional computations are associated with the sensitivities of the vectors involved in the representation of the stochastic load (see Appendix A). Further, since the same excitation model is considered for all reliability constraints, this analysis needs to be performed once to evaluate the sensitivities of all active constraints. For conciseness, only the results corresponding to the final design of case A are presented here. However, additional calculations indicate that similar results are obtained for cases B and C.

For reference purposes, Figure 10 presents the evolution, in terms of the number of samples, of the estimates of $\frac{\partial P_{F_{10}}}{\partial \Omega_1}$ and $\frac{\partial P_{F_{10}}}{\partial \Omega_2}$ evaluated at the final design of Case A (see Table 6). Rather stable estimates are obtained for $N \geq 3000$, with $\frac{\partial P_{F_{10}}}{\partial \Omega_1} \approx -1.70 \times 10^{-2}$ and $\frac{\partial P_{F_{10}}}{\partial \Omega_2} \approx -0.03 \times 10^{-2}$. Thus, in this case $P_{F_{10}}(\mathbf{x})$ is much more sensitive to Ω_1 than to Ω_2. Moreover, increasing the values of Ω_1 or Ω_2 tends to decrease the likelihood of exceeding the maximum allowable threshold in the 10^{th} story. Validation calculations indicate that a similar behavior is also observed for the failure probability functions $P_{F_9}(\mathbf{x})$ and $P_{F_{11}}(\mathbf{x})$, which are associated with the active reliability constraints.

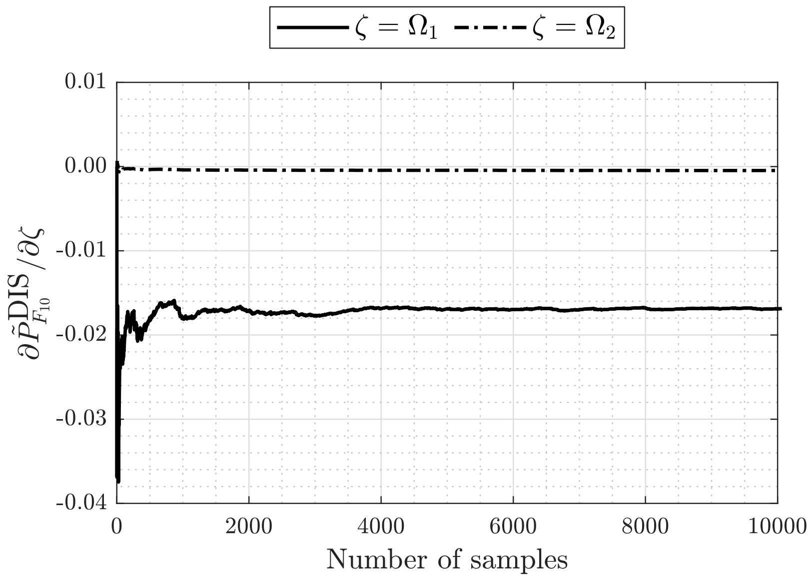

Figure 10: Sensitivity estimates of $P_{F_{10}}$ with respect to Ω_1 and Ω_2 in terms of the number of samples. Scenario II.

Table 8 presents the optimum design sensitivity measures corresponding to perturbations in $\zeta = \Omega_1$ and $\zeta = \Omega_2$, i.e., the sensitivities of the optimum values for the design variable, $\frac{\partial x_i^*}{\partial \zeta}$, $i = 1, \ldots, 8$, and of the optimum objective value, $\frac{df^*}{d\zeta}$. For convenience, all these quantities have been normalized in such a way that the maximum magnitude of the sensitivities of the optimum objective values equals one. From the table, it is seen that the final solution is more sensitive to Ω_1 than to Ω_2, since $\left|\frac{df^*}{d\Omega_1}\right| > \left|\frac{df^*}{d\Omega_2}\right|$. Such behavior, in turn, can be associated with the higher sensitivity of the active reliability constraint functions with respect to this parameter (see Fig. 10). Furthermore, the previous results, which are obtained from the solution of Eq. (15), correspond to perturbations $\delta\Omega_1 > 0$ and $\delta\Omega_2 > 0$. In other words, improved designs can be obtained for larger values of the filter parameters Ω_1 or Ω_2. This agrees with the results presented in Fig. 10. Finally, regarding the rates of change of the optimum values for the design variables with respect to both excitation model parameters, all values in the table are negative. For small changes in Ω_1, the optimum design tends to move almost parallel to the steepest descent direction of the objective function. Meanwhile, a different behavior is observed for perturbations in Ω_2, where core wall thicknesses of upper floors are decreased to a greater extent than the rest. This can be related to the smaller influence of these structural properties on the responses involved in the definition of the active constraint functions, i.e., the drifts of stories 9 to 11.

Based on the previous discussion, it is seen that the optimum design sensitivity approach adopted in this contribution can provide non-trivial information about the effect of model pa-

	$\zeta = \Omega_1$	$\zeta = \Omega_2$
$\partial x_1^*/\partial\zeta$	-0.999	-0.038
$\partial x_2^*/\partial\zeta$	-0.999	-0.042
$\partial x_3^*/\partial\zeta$	-1.000	-0.052
$\partial x_4^*/\partial\zeta$	-1.001	-0.052
$\partial x_5^*/\partial\zeta$	-1.001	-0.052
$\partial x_6^*/\partial\zeta$	-0.997	-0.022
$\partial x_7^*/\partial\zeta$	-1.001	-0.170
$\partial x_8^*/\partial\zeta$	-1.003	-0.188
$df^*/d\zeta$	-1.000	-0.077

Table 8: Normalized sensitivities of the optimum solution with respect to the excitation model parameters Ω_1 and Ω_2. Case A. Scenario II.

rameter perturbations on final designs. As already pointed out, the required sensitivity measures can be computed as a byproduct of the optimization process by virtue of the reliability sensitivity analysis framework enabled by DIS. Thus, valuable insight for decision-making processes involving linear structural systems subject to Gaussian excitation can be obtained with reduced numerical costs. Overall, the results indicate that the use of DIS allows the implementation of potentially useful tools for a practical and real type of RBO problems.

7. Conclusions

This contribution implements Directional Importance Sampling (DIS) as a general reliability and sensitivity assessment framework for reliability-based optimization (RBO) and optimum design sensitivity analysis of linear structural systems under Gaussian excitation. First-order derivatives of the failure probability, with respect to design variables or general model parameters, can be obtained as a byproduct of the sampling process. This enables effective first-order solution methods for the two types of problems under consideration. On the one hand, a first-order sequential optimization strategy based on an efficient feasible-direction interior-point algorithm is adopted to solve RBO problems. The scheme generates a sequence of feasible designs with improving objective values and, moreover, relatively few optimization cycles are required to obtain greatly improved designs. On the other hand, a direction-finding approach is considered for optimum design sensitivity analysis. In this setting, the rates of change of the optimum objective value and of the optimum values for the design variables with respect to model parameters are computed as a byproduct of the DIS results at the final design. Thus, valuable information on final designs and their sensitivities can be obtained with reduced numerical efforts.

An application example involving a 16-story reinforced concrete building structure subject to ground acceleration modeled as a non-stationary filtered white noise process is addressed to assess the performance of the proposed framework. Structural weight minimization subject to reliability and geometric constraints is studied. In particular, reliability requirements involving serviceability conditions for the interstory drifts are considered. Two alternative scenarios in terms of the number of design variables and reliability constraints are presented. In both cases, the optimization strategy enabled by DIS provides optimum designs in an effective manner. Additionally, significant improvements in the objective values are attained after the initial optimization cycles. Furthermore, numerical results also illustrate the advantages of the adopted framework with respect to a direct finite difference implementation, both in terms of numerical efforts and optimization results. These features are beneficial from a practical viewpoint and highlight the capabilities of DIS in the context of RBO problems. As a byproduct of the optimization results, the sensitivities of the optimum design with respect to response thresholds and excitation model parameters are evaluated. Non-trivial information on how final designs can change under small increases or decreases of model parameters is obtained and, in addition, their relative importance with respect to final solutions can be established. Overall, the results indicate that the general sensitivity analysis framework enabled by DIS provides potentially useful tools for decision-making processes involving linear structural systems subject to Gaussian excitation.

Future research efforts involve the assessment of the framework in more complex structural systems. In these cases, the computational cost of a single structural analysis can be significant and, therefore, parametric reduced-order model techniques can be integrated to reduce the numerical efforts. Another research direction corresponds to the evaluation of different RBO methods, in terms of efficiency and robustness, for the class of problems addressed in this contribution. Some of these topics are currently under consideration.

Acknowledgments

This research is partially supported by ANID (National Agency for Research and Development, Chile) under its program FONDECYT, grant numbers 1200087 and 1180271. Also, this research has been partially supported by ANID and DAAD (German Academic Exchange Service, Germany) under CONICYT-PFCHA/Doctorado Acuerdo Bilateral DAAD Becas Chile/2018-62180007. These supports are gratefully acknowledged by the authors.

A. Sensitivity of minimum demand-to-capacity ratio

A.1. Derivatives with respect to structural parameters

In case ν affects the properties of the structural model, the M^{th} impulse response function in Eq. (8) verifies $\eta_M(t) = \eta_M(t,\nu)$ and $\mathbf{a}_{M,K} = \mathbf{a}_{M,K}(\nu)$. Then, from Eq. (14) it is seen that

$$\frac{\partial c(\nu,\mathbf{u})}{\partial \nu} = -\frac{h_M^*}{(\mathbf{a}_{M,K}(\nu)^T\mathbf{u})\,|\mathbf{a}_{M,K}(\nu)^T\mathbf{u}|} \times \left(\left(\frac{\partial \mathbf{a}_{M,K}(\nu)}{\partial \nu} \right)^T \mathbf{u} \right) \tag{24}$$

with

$$\frac{\partial \mathbf{a}_{M,K}(\nu)}{\partial \nu} = \sum_{q=1}^{K} \varepsilon_q \Delta t \frac{\partial \eta_M(t_K - t_q, \nu)}{\partial \nu} \boldsymbol{\psi}_q \tag{25}$$

where $\frac{\partial \eta_M}{\partial \nu}$ can be obtained applying the chain rule due to the use of modal superposition. This requires the derivatives of the mode shapes and natural frequencies, which are computed using the method presented in [53].

A.2. Derivatives with respect to excitation model parameters

Assume that ν is involved in the definition of the stochastic excitation model. Hence, $\mathbf{a}_{M,K} = \mathbf{a}_{M,K}(\nu)$ and, therefore, Eq. (24) is also valid. However, in this case the first-order derivative of the linear map $\mathbf{a}_{M,K}$ becomes

$$\frac{\partial \mathbf{a}_{M,K}(\nu)}{\partial \nu} = \sum_{q=1}^{K} \varepsilon_q \Delta t \eta_M(t_K - t_q) \frac{\partial \boldsymbol{\psi}_q(\nu)}{\partial \nu} \tag{26}$$

which requires, in turn, the first-order derivatives of the set of vectors $\boldsymbol{\Psi}(\nu) = [\boldsymbol{\psi}_1(\nu), \ldots, \boldsymbol{\psi}_{n_T}(\nu)]$ with respect to ν. From Section 2.2, such sensitivities can be computed as

$$\frac{\partial \boldsymbol{\Psi}(\nu)}{\partial \nu} = \frac{1}{2}\boldsymbol{\Lambda}(\nu)^{-1/2} \left[\frac{\partial \boldsymbol{\Lambda}(\nu)}{\partial \nu} \boldsymbol{\Xi}(\nu)^T + 2\boldsymbol{\lambda}(\nu) \frac{\partial \boldsymbol{\Xi}(\nu)}{\partial \nu}^T \right] \tag{27}$$

The derivatives of the eigenvalues $\boldsymbol{\Lambda}(\nu)$ and eigenvectors $\boldsymbol{\Xi}(\nu)$ of the covariance matrix of the stochastic load, $\boldsymbol{\Sigma}(\nu)$, can be computed using any suitable method; see, e.g., [54, 60].

A.3. Derivatives with respect to response thresholds

Assume that ν corresponds to the s^{th} response threshold, that is, $c(\nu,\mathbf{u}) = c(h_s^*,\mathbf{u})$. Hence, the derivative in Eq. (14) can be computed as

$$\frac{\partial c(h_s^*, \mathbf{u})}{\partial h_s^*} = \begin{cases} \dfrac{c_{M,K}(\mathbf{u})}{h_s^*}, & \text{if } s = M \\ 0, & \text{otherwise} \end{cases} \tag{28}$$

This means that the required derivative is non-zero only if the s^{th} failure response determines the closest failure boundary along the direction $\mathbf{u}$. Finally, it is noted that Eq. (28) involves a single arithmetic operation. Thus, marginal computational efforts are required to evaluate the first-order derivative of the failure probability in this case.

References

[1] R. T. Haftka, Z. Gürdal, Elements of Structural Optimization, Springer Netherlands, 1992.

[2] H. O. Madsen, N. C. Lind, S. Krenk, Methods of Structural Safety, Dover Publications, 2006.

[3] G. M. Atkinson, Stochastic modeling of California ground motions, Bulletin of the Seismological Society of America 90 (2) (2000) 255–274.

[4] D. M. Boore, Simulation of ground motion using the stochastic method, Pure and Applied Geophysics 160 (3) (2003) 635–676.

[5] S. Rezaeian, A. Der Kiureghian, A stochastic ground motion model with separable temporal and spectral nonstationarities, Earthquake Engineering & Structural Dynamics 37 (13) (2008) 1565–1584.

[6] Y. Ding, Y. Peng, J. Li, A stochastic semi-physical model of seismic ground motions in time domain, Journal of Earthquake and Tsunami 12 (03) (2018) 1850006.

[7] K. S. Kumar, T. Stathopoulos, Wind loads on low building roofs: A stochastic perspective, Journal of Structural Engineering 126 (8) (2000) 944–956.

[8] O. Ditlevsen, Stochastic model for joint wave and wind loads on offshore structures, Structural Safety 24 (2-4) (2002) 139–163.

[9] B. A. Benowitz, G. Deodatis, Simulation of wind velocities on long span structures: A novel stochastic wave based model, Journal of Wind Engineering and Industrial Aerodynamics 147 (2015) 154–163.

[10] J. Chen, Y. Song, Y. Peng, P. D. Spanos, Simulation of homogeneous fluctuating wind field in two spatial dimensions via a joint wave number-frequency power spectrum, Journal of Engineering Mechanics 144 (11) (nov 2018).

[11] G. A. Athanassoulis, C. N. Stefanakos, A nonstationary stochastic model for long-term time series of significant wave height, Journal of Geophysical Research 100 (C8) (1995) 16149.

[12] G. I. Schuëler, H. A. Jensen, Computational methods in optimization considering uncertainties – An overview, Computer Methods in Applied Mechanics and Engineering 198 (1) (2008) 2–13.

[13] I. Enevoldsen, J. D. Sørensen, Reliability-based optimization in structural engineering, Structural Safety 15 (3) (1994) 169–196.

[14] I. Petromichelakis, A. F. Psaros, I. A. Kougioumtzoglou, Stochastic response analysis and reliability-based design optimization of nonlinear electromechanical energy harvesters with fractional derivative elements, ASCE-ASME Journal of Risk and Uncertaintanty in Engineering Systems, Part B: Mechanical Engineering 7 (1) (jan 2021).

[15] A. G. Carlon, R. H. Lopez, L. F. R. Espath, L. F. F. Miguel, A. T. Beck, A stochastic gradient approach for the reliability maximization of passively controlled structures, Engineering Structures 186 (2019) 1–12.

[16] Y. Peng, Y. Ma, T. Huang, D. D. Domenico, Reliability-based design optimization of adaptive sliding base isolation system for improving seismic performance of structures, Reliability Engineering & System Safety 205 (2021) 107167.

[17] J. Ching, Y.-H. Hsieh, Approximate reliability-based optimization using a three-step approach based on subset simulation, Journal of Engineering Mechanics 133 (4) (2007) 481–493.

[18] J. Wang, L. S. Katafygiotis, Reliability-based optimal design of linear structures subjected to stochastic excitations, Structural Safety 47 (2014) 29 – 38.

[19] H. Yu, F. Gillot, M. Ichchou, Reliability based robust design optimization for tuned mass damper in passive vibration control of deterministic/uncertain structures, Journal of Sound and Vibration 332 (9) (2013) 2222–2238.

[20] W.-S. Liu, S. H. Cheung, Reliability based design optimization with approximate failure probability function in partitioned design space, Reliability Engineering & System Safety 167 (2017) 602 – 611.

[21] K. M. Zuev, J. L. Beck, Global optimization using the asymptotically independent Markov sampling method, Computers & Structures 126 (2013) 107 – 119.

[22] D. J. Jerez, H. A. Jensen, M. Beer, Reliability-based design optimization of structural systems under stochastic excitation: An overview, Mechanical Systems and Signal Processing 166 (2022) 108397.

[23] M. F. Huang, C. M. Chan, W. J. Lou, Optimal performance-based design of wind sensitive tall buildings considering uncertainties, Computers & Structures 98-99 (2012) 7–16.

[24] D. Honfi, A. Mårtensson, S. Thelandersson, Reliability of beams according to Eurocodes in serviceability limit state, Engineering Structures 35 (2012) 48–54.

[25] S. M. J. Spence, M. Gioffrè, Large scale reliability-based design optimization of wind excited tall buildings, Probabilistic Engineering Mechanics 28 (2012) 206–215.

[26] S. M. J. Spence, M. Gioffrè, A. Kareem, An efficient framework for the reliability-based design optimization of large-scale uncertain and stochastic linear systems, Probabilistic Engineering Mechanics 44 (2016) 174 – 182.

[27] S. M. J. Spence, Optimization of uncertain and dynamic high-rise structures for occupant comfort: An adaptive kriging approach, Structural Safety 75 (2018) 57–66.

[28] A. Suksuwan, S. M. J. Spence, Efficient approach to system-level reliability-based design optimization of large-scale uncertain and dynamic wind-excited systems, ASCE-ASME Journal of Risk and Uncertainty in Engineering Systems, Part A: Civil Engineering 4 (2) (2018) 04018013.

[29] S. K. Au, J. L. Beck, First excursion probabilities for linear systems by very efficient importance sampling, Probabilistic Engineering Mechanics 16 (3) (2001) 193–207.

[30] L. Katafygiotis, S. H. Cheung, Domain Decomposition Method for calculating the failure probability of linear dynamic systems subjected to Gaussian stochastic loads, Journal of Engineering Mechanics 132 (5) (2006) 475–486.

[31] M. A. Valdebenito, P. Wei, J. Song, M. Beer, M. Broggi, Failure probability estimation of a class of series systems by multidomain Line Sampling, Reliability Engineering & System Safety 213 (2021) 107673.

[32] M. A. Misraji, M. A. Valdebenito, H. A. Jensen, C. F. Mayorga, Application of directional importance sampling for estimation of first excursion probabilities of linear structural systems subject to stochastic Gaussian loading, Mechanical Systems and Signal Processing 139 (2020) 106621.

[33] A. Der Kiureghian, The geometry of random vibrations and solutions by FORM and SORM, Probabilistic Engineering Mechanics 15 (1) (2000) 81–90.

[34] M. A. Valdebenito, M. A. Misraji, H. A. Jensen, C. F. Mayorga, Sensitivity estimation of first excursion probabilities of linear structures subject to stochastic Gaussian loading, Computers & Structures 248 (2021) 106482.

[35] H. A. Jensen, L. G. Becerra, M. A. Valdebenito, On the use of a class of interior point algorithms in stochastic structural optimization, Computers & Structures 126 (2013) 69–85.

[36] J. Herskovits, G. Santos, On the computer implementation of feasible direction interior point algorithms for nonlinear optimization, Structural optimization 14 (2) (1997) 165–172.

[37] G. N. Vanderplaats, N. Yoshida, Efficient calculation of optimum design sensitivity, AIAA Journal 23 (11) (1985) 1798–1803.

[38] N. Hoang, Y. Fujino, P. Warnitchai, Optimal tuned mass damper for seismic applications and practical design formulas, Engineering Structures 30 (3) (2008) 707–715.

[39] M. J. Tait, Modelling and preliminary design of a structure-TLD system, Engineering Structures 30 (10) (2008) 2644–2655.

[40] R. O. Ruiz, D. Lopez-Garcia, A. A. Taflanidis, Modeling and experimental validation of a new type of tuned liquid damper, Acta Mechanica 227 (11) (2016) 3275–3294.

[41] F. Gomez, B. F. Spencer, Topology optimization framework for structures subjected to stationary stochastic dynamic loads, Structural and Multidisciplinary Optimization 59 (3) (2018) 813–833.

[42] C. Su, B. Li, T. Chen, X. Dai, Stochastic optimal design of nonlinear viscous dampers for large-scale structures subjected to non-stationary seismic excitations based on dimension-reduced explicit method, Engineering Structures 175 (2018) 217–230.

[43] C. A. Schenk, G. I. Schuëller, Uncertainty assessment of large finite element systems, Springer-Verlag, 2005.

[44] G. Stefanou, The stochastic finite element method: Past, present and future, Computer Methods in Applied Mechanics and Engineering 198 (9-12) (2009) 1031–1051.

[45] G. I. Schuëller, H. J. Pradlwarter, P. S. Koutsourelakis, A critical appraisal of reliability estimation procedures for high dimensions, Probabilistic Engineering Mechanics 19 (4) (2004) 463–474.

[46] G. I. Schuëller, H. J. Pradlwarter, Benchmark study on reliability estimation in higher dimensions of structural systems - An overview, Structural Safety 29 (3) (2007) 167 – 182.

[47] A. D. Belegundu, T. R. Chandrupatla, Optimization concepts and applications in engineering, Cambridge University Press, 2011.

[48] A. Chopra, Dynamics of structures: Theory and applications to earthquake engineering, Pearson, Hoboken, NJ, 2017.

[49] W. Gautschi, Numerical analysis, Birkhäuser, Boston, 2012.

[50] O. Ditlevsen, R. Olesen, G. Mohr, Solution of a class of load combination problems by directional simulation, Structural Safety 4 (2) (1986) 95–109.

[51] P. Bjerager, Probability integration by Directional Simulation, Journal of Engineering Mechanics 114 (8) (1988) 1285–1302.

[52] J. Nie, B. R. Ellingwood, Directional methods for structural reliability analysis, Structural Safety 22 (3) (2000) 233–249.

[53] I.-W. Lee, G.-H. Jung, An efficient algebraic method for the computation of natural frequency and mode shape sensitivities—Part I Distinct natural frequencies, Computers & Structures 62 (3) (1997) 429–435.

[54] R. B. Nelson, Simplified calculation of eigenvector derivatives, AIAA Journal 14 (9) (1976) 1201–1205.

[55] G. N. Vanderplaats, An efficient feasible directions algorithm for design synthesis, AIAA Journal 22 (11) (1984) 1633–1640.

[56] G. Vanderplaats, Numerical optimization techniques for engineering design: with applications, McGraw-Hill, New York, 1984.

[57] A. Zerva, Spatial variation of seismic ground motions: modeling and engineering applications, CRC Press, Boca Raton, FL, 2009.

[58] P. A. Hidalgo, C. A. Ledezma, R. M. Jordan, Seismic behavior of squat reinforced concrete shear walls, Earthquake Spectra 18 (2) (2002) 287–308.

[59] J. C. Spall, Introduction to Stochastic Search and Optimization, John Wiley & Sons, Inc., 2003.

[60] R. M. Lin, J. E. Mottershead, T. Y. Ng, A state-of-the-art review on theory and engineering applications of eigenvalue and eigenvector derivatives, Mechanical Systems and Signal Processing 138 (2020) 106536.